Green Chemistry

PAPER

View Article Online
View Journal | View Issue

Cite this: *Green Chem.*, 2025, **27**, 13480

Uniformly crosslinked algal bioplastic with triggerable decomposition in salt water

Andrew E. Ashmar, [a,d] Eric J. Beckman [a,b] and Susan K. Fullerton-Shirey *[a,c]

Addressing marine pollution caused by single-use plastic waste has become an important sustainability goal for preventing ecological hazards caused by microplastics. This work focuses on the reversible crosslinking of dehydrated, sodium alginate plastic films and their selective degradation in seawater into benign byproducts. Films are crosslinked by divalent ions, Ca^{2+} and Sr^{2+}, *via* the hydrolysis of $CaCO_3$ and $SrCO_3$ by glucono-δ-lactone. The rate of Ca^{2+} release in simulated seawater (3.5 wt% NaCl) is quantified as a function of initial Ca^{2+} concentration. At the highest crosslinking densities, there is a seven-fold increase in the amount of Ca^{2+} released in the presence of salt water compared to DI water. Moreover, the calcium release rate increases more strongly with crosslinking density in salt water than DI water, showing that saltwater promotes the reversible crosslinking of the film into alginate salts that are fully soluble in water. Mechanical properties including elastic modulus and ultimate strength, show improvement with crosslinking density until the ion saturation concentration at which point both properties decrease abruptly. Reversible and selective crosslinking is not limited to Ca^{2+}, but extends to other divalent ions including Sr^{2+}, which is also demonstrated. Broadly, these results illustrate how noncovalent interactions in naturally occurring biomaterials can be used to create more sustainable plastics with tunable mechanical properties.

Received 6th June 2025,
Accepted 3rd October 2025

DOI: 10.1039/d5gc02866c

rsc.li/greenchem

Green foundation

1. This work addresses single-use plastic pollution in marine environments by advancing our understanding of how polyelectrolytes can be employed to produce materials that reversibly crosslink in specific environments.
2. We demonstrate how noncovalent interactions in naturally occurring biomaterials can be used to create plastic films that triggerably degrade into benign components in seawater, but stay intact in deionized water.
3. Future research will focus on decreasing the water vapor permeability of the films, and tuning the mechanical properties.

1 Introduction

Single-use plastic pollution in marine environments poses a wide-reaching sustainability risk that is not adequately addressed by current biodegradable plastic technologies. Single-use plastics have become increasingly prevalent in modern society, mainly due to their low cost and durability.[1] However, this resistance to degradation has resulted in significant accumulation of plastic in the ambient environment.[2] These plastic pollutants are incidentally consumed by many organisms, causing direct harm or death.[1] For instance, at least 26% of marine fish have ingested plastic pollutants, which have been shown to cause observable behavioral changes and nervous system damage.[3,4] Ecological hazards from plastic waste are especially prevalent in marine environments, where pollutants have increased mobility and interact with a uniquely complex ecosystem.

Macroplastics—plastic pollutants greater than 5 mm in diameter—are the most conspicuous form of marine plastic pollution. Macroplastics primarily harm marine organisms through inadvertent consumption, as plastics are visually and olfactorily similar to food consumed by many marine organisms, such as sea turtles, seabirds, and fish.[5–7] Although the risks of macroplastic pollution are significant, recent work has drawn attention to the threat of macroplastic degradants called microplastics. Microplastics are synthetic plastic particles less than 5 mm in diameter[8,9] that can penetrate biologi-

[a]*Department of Chemical & Petroleum Engineering, University of Pittsburgh, Pittsburgh, PA 15213, USA. E-mail: fullerton@pitt.edu*
[b]*Mascaro Center for Sustainable Innovation, University of Pittsburgh, Pittsburgh, PA 15213, USA*
[c]*Department of Electrical and Computer Engineering, University of Pittsburgh, Pittsburgh, PA 15213, USA*
[d]*Department of Chemical Engineering, Carnegie Mellon University, Pittsburgh, PA 15213, USA*

cal barriers and cause toxic effects such as reducing fertility, stunting growth, and altering feeding patterns.[10] These effects are likely to become increasingly prevalent, as current estimates suggest that there will be more plastic than fish in the ocean (on a per-mass basis) by 2050.[11] It is imperative that more degradable alternatives to traditional petroleum-derived plastics be developed to protect the integrity of marine ecosystems.

The past decade has brought about many advancements in sustainable plastic technology, especially in the form of so-called "biodegradable plastics" such as polylactic acid (PLA). Although biodegradable plastics are an important step towards reducing the accumulation of plastic waste, they have shortcomings. The biodegradability of a polymer depends on its degradation environment, so technical standards for quantifying biodegradability typically assume disposal in an industrial composter.[12,13] These test conditions do not accurately simulate disposal in an uncontrolled environment, such as the ocean, where plastic pollution can have the most significant ecological impact.[14] demonstrated that biodegradable polymers PLA, polycaprolactone (PCL), and polybutylene adipate terephthalate (PBAT) showed little to no degradation after one year in a simulated marine environment.[14] Further, a meta-analysis suggests that time it takes for a plastic bag made of PLA to degrade to 50% its mass in a marine environment is similar to that of polyethylene: tens to hundreds of years.[15] This is unsurprising, as PLA is insoluble in water.[16]

There are few fully commercialized biodegradable plastics, with most of them limited in their mechanical properties. For example, plastics made from PLA or polyhydroxyalkanoates (PHAs) are known to be brittle with low impact strength.[17,18] Manufacturers have enhanced these properties by blending synthetic polymers with biodegradable polymers; however, recent evidence suggests these polymer blends are more prone to fragmentation into microplastics.[19] The aforementioned limitations of current biodegradable plastics highlight the need for novel, bio-based polymeric materials that rapidly degrade into benign byproducts in a broad range of environments.

The present work demonstrates the use of sodium alginate, a water-soluble, naturally-occurring algal polysaccharide, as a mechanically tunable plastic material that utilizes principles of equimolar counterdiffusion to reversibly crosslink into benign byproducts in seawater. Chemically, sodium alginate is a copolymer consisting of 1,4-linked sequences of monomeric isomers α-L-guluronate (G) and β-D-mannuronate (M), shown in Fig. 1. The dyadic composition of the polymer influences the mechanical properties of the chain, with rigidity increasing in the order MG < MM < GG.[20] Each repeat unit contains a carboxylate unit when pH $\gtrsim$4, making alginate an anionic polyelectrolyte. This polyanionic character, combined with the stereochemical configuration of the repeat units, allows alginate to effectively chelate neighboring cations.[21,22] When the carboxylate moiety is stabilized by a sodium cation, the polymer forms a water-soluble hydrogel. When a polyvalent cation is present, however, neighboring alginate chains link

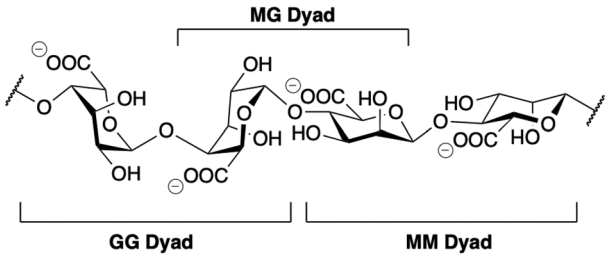

Fig. 1 Dyadic subunits of alginates, comprised of monomers α-L-guluronate (G) and β-D-mannuronate (M).

together to form a mechanically robust polymer network that is insoluble in water and most organic solvents. The affinity of the polyanion for divalent cations—and therefore the strength of the crosslink junctions—generally increases with the steric bulk of the cation.[23] The dyadic composition of the chain also influences its ion-affinity, with the diaxially linked GG subunits most involved in chelation.[22] Crosslink junctions are formed by GG subunits on two neighboring chains that interact with a single divalent cation in what has been called an "egg-box" formation (see Fig. 2).[24,25]

Alginate networks are well-studied because they are frequently used as a biocompatible structural material for tissue engineering.[26] For this reason, most alginate research and applications have focused on the material in its hydrogel form. Of the reports on dehydrated SA films, few are crosslinked by a divalent salts[27–30] and of those, all but one incorporates glycerol as a plasticizer, making the films more hygroscopic. There are no reports of degradation properties in salt water; although, Gubitosa *et al.*, observe film swelling in the presence of monovalent salts.[27] In this work, we report on dehydrated alginate films crosslinked with Ca^{2+}, and demonstrate their selective degradation and total dissolution when Ca^{2+} is exchanged with Na^{+} in salt water. The rate of Ca^{2+} release in salt *versus* deionized water is quantified, showing a nearly seven fold increase at the highest crosslinking concentration which leads to total dissolution of the film. Prior work suggests that microorganisms in a marine environment could further accelerate this degradation.[31] We also demonstrate how the mechanical properties of the material can be tuned by

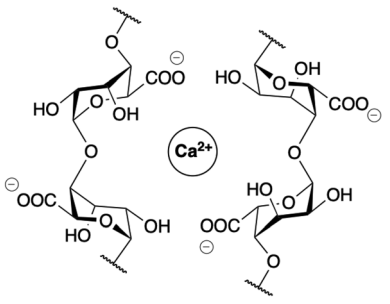

Fig. 2 Calcium-mediated alginate "egg-box" crosslink junctions formed by GG dyads. Adapted from ref. 24.

modifying the identity and/or concentration of the crosslinking ion. At a low concentration of crosslinking cations, increasing the crosslinker concentration increases mechanical strength and reduces flexibility. However, as the crosslinker concentration is further increased, the films become mechanically weaker and more flexible. These results suggest that alginate-based materials could be used as a triggerably degradable bio-derived replacement for traditional petroleum-derived plastics. More broadly, this work illustrates how noncovalent interactions in naturally occurring biomaterials can be utilized to create more sustainable plastic materials with tunable mechanical properties.

2 Experimental

2.1 Source polymer characterization

2.1.1 Molecular weight. Powdered sodium alginate of varying viscosities were purchased from Sigma-Aldrich (Lot A) and Fisher Scientific (Lot B). Molecular weight was quantified *via* intrinsic viscosity measurements using a 75 Cannon-Fenske viscometer and the Mark–Houwink parameters K = 0.00504 and a = 1.01.[32,33] The viscosity-average molecular weight determined by the Mark–Houwink equation is equivalent to the weight-average molecular weight because $a \approx 1$. Details of the measurement are provided in section 1 of the SI.

2.1.2 Dyadic composition. Dyadic composition of each alginate lot was determined using circular dichroism spectroscopy as described by Donati and coworkers.[34] Briefly, aqueous samples of each alginate sample were prepared at a concentration of 1 g L^{-1}. Samples were placed in a cuvette of pathlength 0.5 cm and analyzed in triplicate using an Olis 17 UV/Vis/NIR spectrophotometer. Nonlinear least-squares regression was used to estimate the dyadic composition of each sample using data from ref. 34. Additional details describing the data collection and analysis are provided in section 2 of the SI.

2.2 Alginate film preparation

Samples from each alginate lot were dissolved in MilliQ grade deionized water under variable shear agitation to a final concentration of 10 wt%. The alginate solution was crosslinked with either calcium or strontium *in situ via* the rate-limited hydrolysis of $CaCO_3$ or $SrCO_3$ by glucono-δ-lactone (GDL).[35,36] The carbonate salt was sonicated in water and immediately added to the alginate solution. A freshly prepared aqueous solution of GDL was added to the alginate solution containing the carbonate salt to form a 2 : 1 molar ratio of GDL to $CaCO_3$/$SrCO_3$. The amount of carbonate salt added was varied based to target specific molar ratios of divalent cation to alginate repeat units. Samples were prepared at varying crosslink densities, measured in monomoles† of divalent cation. The alginate solution was immediately agitated after the addition of GDL and formed into a thin film (25–50 μm) on a high-density polyethylene substrate using a wire-wound stainless steel Mayer rod (size 75). The film was allowed to dry overnight at room temperature. Once dry, the microstructure of each film was optically inspected using a Zeiss Axio Lab A1 microscope equipped with a dark-field condenser lens. Film thickness was quantified using an ultrasonic thickness gauge, with most films measuring *ca.* 30 μm. Additional details of the GDL reaction and film preparation are provided in section 3 of the SI.

2.3 Film degradation

Degradation of the alginate films was characterized by placing films of constant thickness and known mass in solutions containing either deionized water or 3.5 wt% NaCl for seven days at room temperature. Note that thermal decomposition of alginate occurs at T > 200 °C.[37] Samples were lightly agitated on a shaker table at 100 rpm to simulate wave action. The degradation rate was quantified by measuring the concentration of calcium ions in the surrounding water at discrete time points using ion-coupled plasma optical emission spectroscopy (ICP-OES). Aqueous samples were acidified with 1 M HNO_3 prior to ICP-OES analysis. Ion concentration measurements were normalized based on the mass of the film in solution. All degradation experiments were completed in triplicate. Additional detailed of the mass spec measurements are provided in section 4 of the SI.

2.4 Mechanical characterization

Mechanical properties of the films were measured using a uniaxial tensile test at room temperature, where the films are in the glassy state. The glass transition temperature of dry alginate films ranges from 119–130 °C depending on crosslinking conditions and isomeric composition.[37] The samples were cut in a dog bone shape with an overall length of 35 mm, a gauge length of 15 mm, and a width of 3 mm. The thickness of each sample was measured using an ultrasonic thickness gauge. Before testing, samples were equilibrated at approximately 40% relative humidity. Testing was performed in triplicate using an Instron Universal Testing Machine (Model 4442) at a strain rate of 0.50 mm min^{-1}, continuing until sample fracture. All experiments were repeated in triplicate. Data treatment, provided in section 5 of the SI, was performed according to ASTM D638.[38] The values of the elastic modulus and ultimate strength were calculated for each sample.

2.5 Water contact angle

Film hydrophobicity was quantified using water contact angle measurements recorded using a VCA Optima video contact angle system. Before water contact angle measurements, samples were equilibrated at approximately 40% relative humidity. The test was performed by dispensing 1 μL of deionized water on the surface of the film. A microscopic image was taken of the droplet on the film, and software was used to measure the contact angle. Each experiment was repeated in triplicate to confirm reproducibility.

†A monomole is equivalent to one mole of reactant per molar equivalent of monomer present in the polymer.

3 Results & discussion

3.1 Molecular weight and chemical composition

The weight-average molecular weight, quantified by measurements of the intrinsic viscosity, are reported in Table 1. Lot A is 85 000 g mol^{-1} and Lot B is 180 000 g mol^{-1}. Also reported in Table 1 are the frequency of each monad and dyad, expressed on a fractional basis, measured by circular dichroism spectroscopy. Lot A has a considerably larger fraction of GG dyads (F_{GG} = 0.521) than Lot B (F_{GG} = 0.224), suggesting that Lot A will more readily bind to divalent cations.

3.2 Optical analysis of dried films

The microstructure of each film was examined under a light microscope equipped with a dark-field condenser lens. This lens was chosen to highlight imperfections in the film that could affect the bulk mechanical properties of the material. Microscopic images of films prepared using Lots A and B, both uncrosslinked and crosslinked with 0.125 monomol Ca^{2+} are shown in Fig. 3. The uncrosslinked alginate films from both Lot A and Lot B appear mostly homogeneous, with few imperfections present. The crosslinked films from Lot A appear mostly homogeneous, while films prepared from Lot B exhibit significant macrophase separation. Creating films with only GDL (*i.e.*, without $CaCO_3$) confirm the crystalline features as $CaCO_3$.

Table 1 Chemical properties of sodium alginate samples used to form cross-linked films

Lot ID	M_w (g mol^{-1})	F_G	F_M	F_{GG}	F_{MM}	F_{MG}
A	85 000	0.636	0.364	0.521	0.247	0.232
B	180 000	0.396	0.604	0.224	0.433	0.323

F denotes the fractional composition of each monad and dyad.

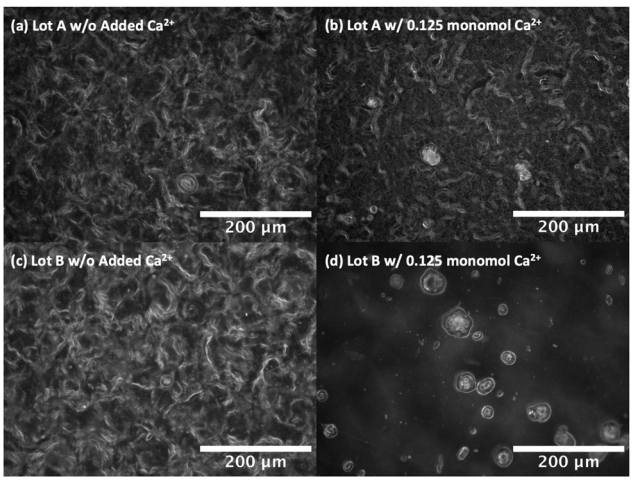

Fig. 3 Dark-field microscopy images of films prepared using (a) Lot A with no added calcium, (b) Lot A with 0.125 monomol Ca^{2+}, (c) Lot B with no added calcium, and (d) Lot B with 0.125 monomol Ca^{2+}. Additional microscopy images can be found in the Fig. S3, S4, and S6.

The presence of $CaCO_3$ precipitate in films from Lot B—and not films from Lot A—suggests that phase separation depends on the dyadic composition of the alginate chain. According to the traditional egg-box model, the maximum amount of calcium that can bind to an alginate network is equal to one-half the molar fraction of GG dyads.[25] In other words, each divalent cation requires two GG dyads to form the theorized egg-box structure. Because alginate from Lot A contains twice the number of GG dyads than Lot B, it is reasonable to expect Lot A to bind more Ca^{2+} than Lot B, and therefore show less undissolved $CaCO_3$ at the same calcium concentration. We hypothesize that when the anionic binding sites on the alginate chain are fully saturated with calcium cations, excess calcium ions remain bound to the carbonate counterions resulting in phase separation in the bulk material. To explore this hypothesis, films with a range of Ca^{2+} concentrations are prepared from each alginate lot. To identify the concentration at which Lot B films became optically homogeneous, films were prepared with calcium concentrations decreasing incrementally from 0.125 monomol Ca^{2+} to 0.050 monomol Ca^{2+}. As the calcium content decreased, film inhomogeneity also decreased until 0.050 monomol Ca^{2+}, at which point the films appeared mostly homogeneous under an optical microscope (Fig. S3). Note that 0.050 monomol Ca^{2+} corresponds to about half of the theoretical maximum calcium concentration for Lot B, which is $F_{GG}/2$ = 0.112 monomol.

For Lot A, the calcium concentration was increased from 0.125 to 0.250 and 0.375 monomol Ca^{2+}. Both concentrations showed phase separation, suggesting optical homogeneity is limited to concentrations less than 0.125 monomol Ca^{2+}. Similar to Lot B, optical homogeneity is observed at approximately one half the theoretical maximum for Lot A, which is $F_{GG}/2$ = 0.26 monomol (Fig. S4).

It is worth nothing that our solid-state films exhibit phase separation, as detectable by optical microscopy, at a calcium concentrations equal to one half the stoichiometric maximum of two GG to one Ca^{2+}. One possible explanation for the discrepancy is the high density of polymer chains in our films compared to those of hydrogels and dilute solutions. Initial experiments describing the egg-box model used dilute polymer solutions,[25] which optimize chain mobility and promote dimerization. Because our films contain a much higher concentration of polymer chains, mobility of both the polymer and Ca^{2+} are limited making it less favorable for GG-dyads to rearrange and form egg-box constructs. The limited number of favorable conformational positions for stable alginate–cation complexes ultimately limits the amount of calcium that can bind to the polymer, leaving some $CaCO_3$ unsolubilized. This inhomogeneity is important because it significantly affects the physical properties of the polymer network, as reported below in section 3.4.

3.3 Film degradation properties

Degradation in the ocean was simulated by immersing the alginate films in an aqueous solution of 3.5 wt% NaCl for seven days. An identical film was placed in MilliQ-grade de-

ionized water to serve as a control. The degree of degradation was quantified by measuring the concentration of dissolved calcium in the aqueous layer *via* ICP-OES. Data were normalized based on the mass of alginate film entering the solution. Fig. 4 reports the normalized concentration of dissolved calcium as a function of time for the uncrosslinked, 0.125, 0.250 and 0.375 monomol Ca^{2+} concentrations.

The amount and rate at which calcium ions are released is a reliable indicator of the material's degradation rate, because calcium ions are responsible for crosslinking the polymer network. Focusing first on samples placed in deionized water, the rate of Ca^{2+} release increases slightly with crosslink density, with films containing 0.375 monomol Ca^{2+} releasing calcium approximately 1.2 times faster than samples containing 0.125 monomol Ca^{2+}. However, in a simulated seawater environment, the rate of calcium release is much higher than in DI water, and it is more strongly correlated with crosslink density. At the highest concentration of crosslinker (0.375 monomol Ca^{2+}), we measure a seven-fold increase in the amount of Ca^{2+} released compared to in DI water. Moreover, the Ca^{2+} is released 3.2 times faster than films crosslinked at a lower Ca^{2+} concentration (0.125 monomol Ca^{2+}). The stronger correlation between crosslink density and calcium release rate in the simulated seawater compared to DI water suggests that alginate films decrosslink more readily in salt water than in DI water.

These results are corroborated by qualitative observations made throughout the experiment. The uncrosslinked samples dissolved almost immediately after coming into contact with both deionized water and salt water. However, the crosslinked samples swell and eventually fragment in salt water while maintaining their shape in deionized water (see Fig. S5 and the timelapse video provided in the SI). These quantitative and qualitative results suggest that the network can easily reverse its crosslinks in the presence of NaCl, but maintain its integrity in the absence of NaCl.

The faster release of divalent cations in salt water than in deionized water is likely driven by a combination of diffusive and electrostatic forces. From a diffusion perspective, the large concentration gradient between the crosslinked film and the surrounding deionized water will drive the cations to diffuse from the film and into the aqueous solution. However, the anionic character of the alginate polymer induces a Donnan equilibrium in deionized water that likely counteracts the diffusive forces, promoting the retention of divalent cations in the polymer network.

In contrast, the high concentration of sodium cations in salt water leads to an environment that is less favorable for concentration-gradient driven diffusion, but it also creates a Donnan potential that shifts the electrostatic equilibrium and likely permits counterdiffusion of divalent cations to occur at a significant rate. This explanation may account for the robustness of alginate crosslinks in deionized water and their susceptibility to degradation under high salinity conditions. From a practical perspective, such selective degradation is favorable, as it allows the bulk material to maintain its integrity with exposure to deionized water, but readily degrade under prolonged contact with salt water. Another practical consideration is that the degradation rate will vary with temperature in the ocean, with lower water temperatures resulting in slower dissolution. However, given that microplastics of synthetic polymers can take tens or hundreds of years to fully degrade, it is reasonable to expect the dissolution of alginates to occur over shorter timescales.

The degradation rate of strontium-crosslinked films was quantified to understand if and how the identity of the crosslinking cation affects degradation of the bulk material. As shown in Fig. 5, strontium-crosslinked films also degrade more readily in salt water than in deionized water. This is likely due to the same Donnan equilibrium mechanism previously described for calcium-alginate networks. However, our data also shows that strontium-crosslinked films degrade slower than calcium-crosslinked films in both salt water and deionized water. Slower strontium degradation is likely attributable to the stronger binding affinity of strontium–alginate complexes relative to calcium-alginate complexes, which subsequently shifts the Donnan equilibrium in favor of strontium–alginate complexes.[23] The degredation of strontium-crosslinked films is practically relevant because it demonstrates that (1) divalent cations beyond calcium exhibit this be-

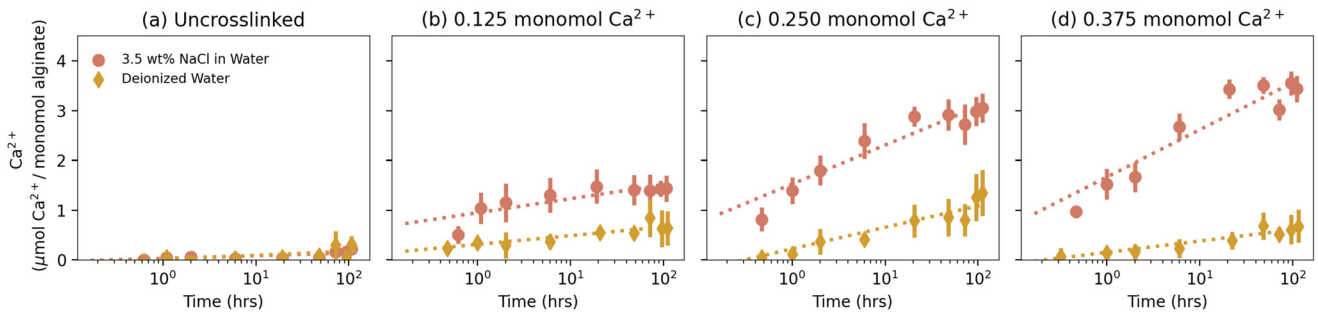

Fig. 4 Concentration of dissolved calcium as a function of film immersion time for films from Lot A (a) uncrosslinked and crosslinked with (b) 0.125 monomol Ca^{2+}, (c) 0.250 monomol Ca^{2+}, and (d) 0.375 monomol Ca^{2+}. Dissolved calcium concentrations obtained from ICP-OES are normalized by the mass of the alginate film. Error bars represent one standard deviation from the mean (n = 3). Dotted lines depict the fitted linear regression models for each dataset.

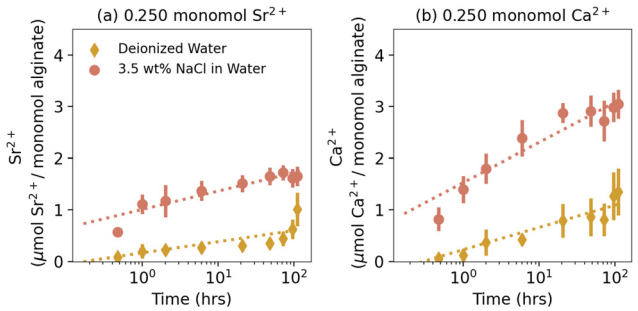

Fig. 5 Concentration of dissolved Sr^{2+} and Ca^{2+} as a function of film immersion time for films crosslinked with (a) 0.250 monomol Sr^{2+} and (b) 0.250 monomol Ca^{2+}. Dissolved cation concentrations obtained from ICP-OES are normalized by the mass of the alginate film. Error bars represent one standard deviation from the mean (n = 3). Dotted lines depict the fitted linear regression models for each dataset.

havior and (2) the durability of alginate-based materials can be adjusted by the choice of crosslinking cation.

3.4 Mechanical properties

We quantified the influence of varying crosslinker identity and concentration on the bulk mechanical properties of the alginate films using uniaxial tensile testing. The elastic modulus, ultimate elongation, and ultimate strength for samples from alginate Lot B prepared at various crosslink densities are shown in Fig. 6, and agree with previous reports.[39,40] The elastic modulus and ultimate strength, (Fig. 6a,c), remain fairly constant up to a concentration of 0.100 monomol Ca^{2+}, after which they decrease by nearly a factor of two at higher concentrations.

Crosslinking is generally expected to enhance the ultimate strength of polymeric materials; however, a two-sample t-test of the data in Fig. 6c reveals no statistically significant difference between the ultimate strength of the uncrosslinked alginate and that of alginate crosslinked with less than 0.115 monomol Ca^{2+}. In contrast, the ultimate elongation of crosslinked samples decreased significantly relative to the control, consistent with crosslink formation (Fig. 6b). We attribute the absence of a significant strengthening effect at low crosslink densities to the presence of undissolved $CaCO_3$, as observed in microscopy images (Fig. S4). Such localized inhomogeneities are known to compromise mechanical integrity and introduce variability in property measurements due to localized crazing at interfacial regions.[41,42] At Ca^{2+} concentrations greater than 0.100 monomol, both the ultimate strength and elastic modulus markedly decrease, which we attribute to phase separation within the material. As discussed previously, the theoretical maximum calcium concentration for Lot B is 0.115 monomol Ca^{2+}, closely corresponding to the concentration at which this abrupt reduction in mechanical properties occurs. Beyond this threshold, significant phase separation between the saturated alginate film and undissolved $CaCO_3$ is evident in Fig. S4. We therefore ascribe the pronounced decrease in elastic modulus and ultimate strength at high Ca^{2+} concentrations to the presence of excess salt remaining in the film after saturation of all GG dyads.

To investigate the impact of cation identity on the mechanical properties of alginate films, films containing 0.050 monomol of Sr^{2+} were prepared and analyzed using uniaxial tensile testing. Fig. 7 presents the mechanical properties of uncrosslinked alginate, alginate crosslinked with 0.050 monomol of Sr^{2+}, and alginate crosslinked with 0.050 monomol of Ca^{2+}. This cation concentration was chosen because it is below the concentration at which the ion-binding capacity is reached. Interestingly, the Sr^{2+} crosslinked sample exhibits a lower ultimate strength and elastic modulus than both the uncrosslinked sample and the sample crosslinked with Ca^{2+}. This is surprising considering Sr^{2+} exhibits a greater binding affinity to alginate than Ca^{2+}.[21] Additionally, upon microscopic examination of both crosslinked films, significant phase separation was only observed in the strontium–alginate material (Fig. S6). We attribute the phase separation in the strontium-crosslinked material to the strong binding affinity between alginate and strontium cations. As strontium strongly

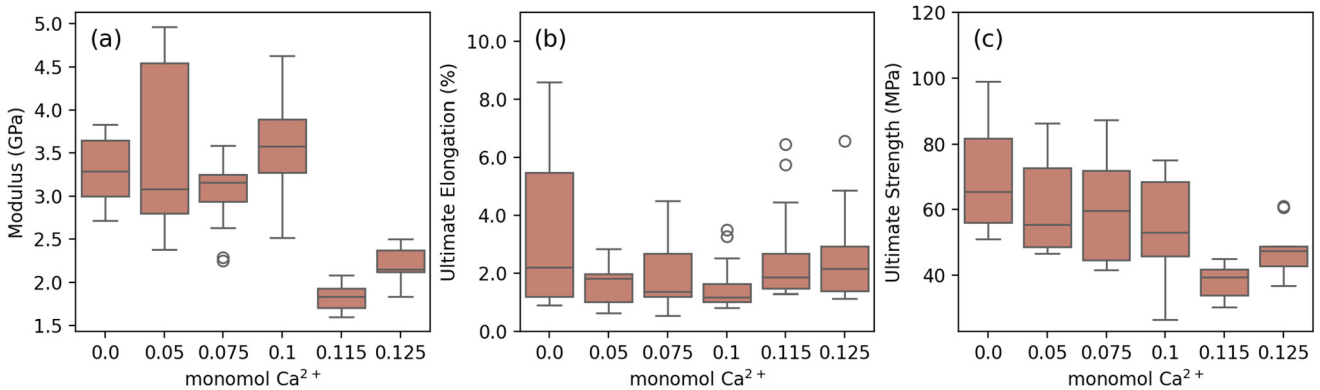

Fig. 6 Mechanical properties. (a) Elastic modulus, (b) ultimate elongation, and (c) ultimate strength as a function of Ca^{2+} crosslink density. Alginate used in these films is from Lot B. The box represents the interquartile range comprising 50% of the data and the bars indicate the maximum and minimum data points.

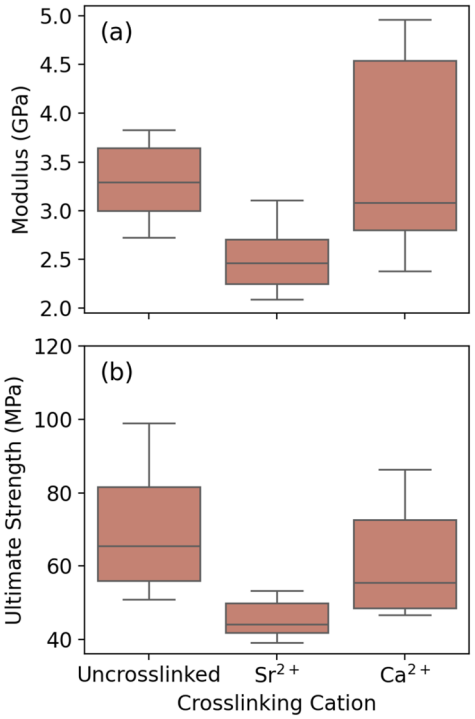

Fig. 7 (a) Elastic modulus and (b) ultimate strength of uncrosslinked alginate, alginate crosslinked with 0.050 monomol Sr^{2+}, and alginate crosslinked with 0.050 monomol Ca^{2+}. All alginate samples are from Lot B.

binds to alginate dyads, it reduces the mobility of the polymer chains much more than calcium, making the formation of strontium–alginate "egg-box" constructs less favorable in the solid state. This would ultimately cause the strontium salt to phase separate from the rest of the material at concentrations well below the stoichiometric maximum. The strontium carbonate that has phase separated from the material likely plasticizes the polymer network, decreasing the strength and elasticity compared to the uncrosslinked material.

Generally speaking, the alginate films prepared using Lot B exhibit mechanical properties comparable to petrochemical-based plastics. At a crosslink density of 0.100 monomol Ca^{2+}, films prepared from Lot B exhibit elastic moduli similar to that of polystyrene.[43] These mechanical properties could theoretically be further tuned by using alginate polymers of different dyadic compositions or molecular weights,[44] or through the use of small-molecule plasticizers such as glycerol.

3.5 Film hydrophilicity

The hydrophobic character of a polymeric material strongly influences its potential applications. To quantify the hydrophilicity of our alginate films, we measured the contact angle between a water droplet and the film surface. Table 2 shows the contact angle measurements for alginate samples from Lots A and B with varying concentrations of Ca^{2+}. A water contact angle could not be determined for the uncrosslinked films from either lot as the water droplet was immediately absorbed by the hydrophilic film.

Table 2 Water droplet contact angle measurements for films prepared from alginate Lots A and B at multiple crosslink densities

Ca^{2+} concentration	Contact angle ± standard deviation (°)
Lot A	
0.125 monomol	34.3° ± 1.5°
0.250 monomol	24.2° ± 1.5°
0.375 monomol	26.9° ± 0.5°
Lot B	
0.050 monomol	37.2° ± 2.0°
0.075 monomol	35.0° ± 1.5°
0.100 monomol	33.3° ± 1.0°
0.115 monomol	26.3° ± 2.0°
0.125 monomol	25.7° ± 1.0°

Each measurement was performed in triplicate. Standard deviations are rounded to the nearest ±0.5°, corresponding to the accuracy of the measurement method.

Water contact-angle measurements on Lot A alginate show that increasing the calcium concentration from 0 to 0.125 monomol significantly increases the contact angle from an unmeasurable value to *ca.* 34.3°. A similar trend was observed for films formed from Lot B. It is not surprising that crosslinking improves film hydrophobicity, as crosslinking is known to make alginate more hydrophobic.[44,45] However, when the concentration increases to 0.250 monomol for Lot A and 0.115 monomol for Lot B, the contact angle decreases, indicating increasing hydrophilicity. As detailed in section 3.2, the estimated ion binding capacity for Lots A and B are 0.26 and 0.112 monomol, respectively, with phase separation becoming observable near these concentrations. Thus, the increased hydrophilicity of the films near these calcium concentrations can likely be attributed to salt concentrations that surpass the polymer networks' ion-binding capacity. Although crosslinking reduces hydrophilic character in alginates,[45] excess salt is likely to make the film more hygroscopic. For example, polymer electrolytes show increasing water concentration with increasing salt concentration.[46] Moreover, crystalline $CaCO_3$ can directly incorporate water into its crystalline structure in the form of hydrates.[47] Thus, once the network becomes fully crosslinked, any additional salt not involved in the crosslinking mechanism likely reduces the hydrophobic character of the material.

Admittedly, the most significant obstacle to the practical application of these films is their hygroscopic behavior. This is the trade-off of when creating a polymer that is mechanically useful and also triggerably degradable in salt water. However, the contact angle measurements, for films equilibrated at 40% relative humidity, demonstrate that it is possible to significantly increase the hydrophobicity of the films through ionic crosslinking. If the unbound salt is contributing to the hydrophillic behavior, then an approach that would significantly reduce the amount of excess salt entrapped in the polymer

network is crosslinking by immersion in a salt solution, which has been previously demonstrated.[27,48] Moving forward, bio-based water vapor barriers that both prevent water uptake while not compromising triggerable dissolution will be explored.

4 Conclusions

With the global accumulation of plastic pollutants increasing at an alarming rate, there is a growing need for alternative plastics that degrade in a wider range of environments, especially in the ocean. We demonstrate the use of solid-state sodium alginate films as a bioplastic that reverses its crosslinks in the presence of seawater. We observe that calcium-crosslinked alginate films reverse their crosslinks in salt water much faster than in deionized water. Unlike PLA, which degrades slowly and can persist as water-insoluble microplastic fragments, our alginate bioplastic rapidly dissolves into naturally occurring, environmentally compatible components in salt water. Although this study focuses on sodium alginate derived from brown algae, the ionic crosslinking strategy demonstrated here could theoretically be adapted to other naturally occurring polyelectrolytes with comparable chelating functionalities.

While alginate is well-studied in its hydrogel form, our work demonstrates some important practical considerations for using alginate in the solid state as a plastic material. Solid-state alginate materials exhibit a reduced ability to bind with divalent cations, likely due to the dense arrangement of chains limiting molecular mobility. When the calcium concentration surpasses an alginate polymer network's ion-binding capacity, phase separation occurs, leading to inferior mechanical and water-repellent properties. While material hydrophilicity remains a concern, we demonstrate that calcium crosslinking significantly increases the hydrophobic character of the material compared to uncrosslinked alginate. These results suggest that sodium alginate has the potential to be used as a readily-degradable marine-friendly bioplastic, provided that the mechanical properties can be engineered to be comparable to petroleum-derived plastics.

Author contributions

Conceptualization: E. J. B., S. K. F.; data curation: A. E. A.; formal analysis: A. E. A.; funding acquisition: E. J. B., S. K. F.; investigation: A. E. A., S. K. F.; methodology: A. E. A.; project administration: S. K. F.; resources: S. K. F.; software; supervision: E. J. B., S. K. F.; validation; visualization; writing – original draft: A. E. A., S. K. F.; writing – review & editing: A. E. A., E. J. B., S. K. F.

Conflicts of interest

There are no conflicts to declare.

Data availability

Additional experimental details, microscopy images, video, and photographic evidence of film degradation are included as part of the supplementary information (SI). Supplementary information is available. See DOI: **https://doi.org/10.1039/d5gc02866c**.

Acknowledgements

The authors gratefully acknowledge the Ellen MacArthur Foundation and Nine Sigma for supporting this work. We also acknowledge undergraduate researchers Sam Landon, Anna Workosky, Samantha Bunke and Jon Bingaman for their contributions, and the Swanson School of Engineering for their support through a Summer Undergraduate Research Internship. We are grateful to Professors Lei Li, Jennifer Laaser, Sachin Velankar, and Daphne WY Chan for providing access to equipment, and to David Malehorn for his expertise and guidance on ICP-OES measurements. The table of contents graphic was created using BioRender.com.

References

1 Y. Chen, A. K. Awasthi, F. Wei, Q. Tan and J. Li, *Sci. Total Environ.*, 2021, **752**, 141772.
2 R. Geyer, J. R. Jambeck and K. L. Law, *Sci. Adv.*, 2017, **3**, e1700782.
3 M. S. Savoca, A. G. McInturf and E. L. Hazen, *Global Change Biol.*, 2021, **27**, 2188–2199.
4 K. Mattsson, E. V. Johnson, A. Malmendal, S. Linse, L.-A. Hansson and T. Cedervall, *Sci. Rep.*, 2017, **7**, 11452.
5 Q. A. Schuyler, C. Wilcox, K. Townsend, B. D. Hardesty and N. J. Marshall, *BMC Ecol.*, 2014, **14**, 14.
6 C. Wilcox, M. Puckridge, Q. A. Schuyler, K. Townsend and B. D. Hardesty, *Sci. Rep.*, 2018, **8**, 12536.
7 M. S. Savoca, M. E. Wohlfeil, S. E. Ebeler and G. A. Nevitt, *Sci. Adv.*, 2016, **2**, e1600395.
8 C. Arthur, J. Baker, H. Bamford, N. Barnea, R. Lohmann, K. McElwee, C. Morishige and R. Thompson, Proceedings of the International Research Workshop on the Occurrence, Effects, and Fate of Microplastic Marine Debris, Tacoma, WA, 2008-09-09/2008-09-11.
9 J. P. G. L. Frias and R. Nash, *Mar. Pollut. Bull.*, 2019, **138**, 145–147.
10 V. G. Mason, M. W. Skov, J. G. Hiddink and M. Walton, *Sci. Total Environ.*, 2022, **845**, 157362.
11 World Economic Forum, *The New Plastics Economy—Rethinking the Future of Plastics*, Ellen MacArthur Foundation and McKinsey & Company, 2016.
12 J. P. Harrison, C. Boardman, K. O'Callaghan, A.-M. Delort and J. Song, *R. Soc. Open Sci.*, 2018, **5**, 171792.
13 T. P. Haider, C. Völker, J. Kramm, K. Landfester and F. R. Wurm, *Angew. Chem., Int. Ed.*, 2019, **58**, 50–62.

14 A. R. Bagheri, C. Laforsch, A. Greiner and S. Agarwal, *Global Challenges*, 2017, **1**, 1700048.
15 A. Chamas, H. Moon, J. Zheng, Y. Qiu, T. Tabassum, J. H. Jang, M. Abu-Omar, S. L. Scott and S. Suh, *ACS Sustainable Chem. Eng.*, 2020, **8**, 3494–3511.
16 N. G. Khouri, J. O. Bahú, C. Blanco-Llamero, P. Severino, V. O. Concha and E. B. Souto, *J. Mol. Struct.*, 2024, **1309**, 138243.
17 K. Hamad, M. Kaseem, H. W. Yang, F. Deri and Y. G. Ko, *eXPRESS Polym. Lett.*, 2015, **9**, 435–455.
18 B. Laycock, P. Halley, S. Pratt, A. Werker and P. Lant, *Prog. Polym. Sci.*, 2013, **38**, 536–583.
19 X.-F. Wei, M. S. Hedenqvist, L. Zhao, A. Barth and H. Yin, *Green Chem.*, 2022, **24**, 8742–8750.
20 O. Smidsrød, R. Glover and S. G. Whittington, *Carbohydr. Res.*, 1973, **27**, 107–118.
21 A. Haug and O. Smidsrød, *Acta Chem. Scand.*, 1970, **24**, 843–854.
22 O. Smidsrød, *Faraday Discuss. Chem. Soc.*, 1974, **57**, 263–274.
23 A. Haug and O. Smidsrød, *Acta Chem. Scand.*, 1965, **19**, 341–351.
24 G. T. Grant, E. R. Morris, D. A. Rees, P. J. Smith and D. Thom, *FEBS Lett.*, 1973, **32**, 195–198.
25 E. R. Morris, D. A. Rees, D. Thom and J. Boyd, *Carbohydr. Res.*, 1978, **66**, 145–154.
26 G. Skjåk-Bræk, I. Donati and S. Paoletti, *Polysaccharide Hydrogels: Characterization and Biomedical Applications*, Pan Stanford, 2016.
27 J. Gubitosa, V. Rizzi, C. Marasciulo, F. Maggi, G. Caprioli, A. M. Mustafa, P. Fini, N. De Vietro, A. M. Aresta and P. Cosma, *Int. J. Mol. Sci.*, 2023, **24**, 11462.
28 H. Zhou, N. Yang, J. Hou, C. Yu, Z. Jin, P. Zeng, L. Yang, Y. Fu, Y. Shen and S. Guo, *Food Packag. Shelf Life*, 2022, **34**, 100935.
29 W. Y. Tong, A. R. Ahmad Rafiee, C. R. Leong, W.-N. Tan, D. J. Dailin, Z. M. Almarhoon, M. Shelkh, A. Nawaz and L. F. Chuah, *Chemosphere*, 2023, **336**, 139212.
30 A. Fasulo, C. Towie, L. Mouchiroud, H. Malik, D. Foucher and G. Sacripante, *Polysaccharides*, 2025, **6**, 20.
31 J. Jacquin, J. Cheng, C. Odobel, C. Pandin, P. Conan, M. Pujo-Pay, V. Barbe, A.-L. Meistertzheim and J.-F. Ghiglione, *Front. Microbiol.*, 2019, **10**, 865.
32 M. R. Cannon and M. R. Fenske, *Ind. Eng. Chem., Anal. Ed.*, 1938, **10**, 297–301.
33 I. M. N. Vold, K. A. Kristiansen and B. E. Christensen, *Biomacromolecules*, 2006, **7**, 2136–2146.
34 I. Donati, A. Gamini, G. Skjåk-Bræk, A. Vetere, C. Campa, A. Coslovi and S. Paoletti, *Carbohydr. Res.*, 2003, **338**, 1139–1142.
35 K. I. Draget, K. Østgaard and O. Smidsrød, *Appl. Microbiol. Biotechnol.*, 1989, **31**, 79–83.
36 K. I. Draget, K. Østgaard and O. Smidsrød, *Carbohydr. Polym.*, 1990, **14**, 159–178.
37 R. Russo, M. Malinconico and G. Santagata, *Biomacromolecules*, 2007, **8**, 3193–3197.
38 ASTM Subcommittee D20.10, *ASTM D638: Standard Test Method for Tensile Properties of Plastics*, 2022.
39 M. Ureña, D. Carullo, T. T.-T. Phùng, P. Fournier, S. Farris, A. Lagorce and T. Karbowiak, *Food Hydrocolloids*, 2024, **149**, 109557.
40 A. S. Giz, M. Berberoglu, S. Bener, S. Aydelik-Ayazoglu, H. Bayraktar, B. E. Alaca and H. Catalgil-Giz, *Int. J. Biol. Macromol.*, 2020, **148**, 49–55.
41 G. H. Michler and H.-H. K.-B. von Schmeling, *Polymer*, 2013, **54**, 3131–3144.
42 R. Protz, N. Kosmann, M. Gude, W. Hufenbach, K. Schulte and B. Fiedler, *Composites, Part B*, 2015, **83**, 346–351.
43 *Polymer Handbook*, ed. J. Brandrup, E. H. Immergut, E. A. Grulke, A. Abe and D. Bloch, Wiley, New York, 4th edn, 1999.
44 K. I. Draget, O. Gåserød, I. Aune, P. O. Andersen, B. Storbakken, B. T. Stokke and O. Smidsrød, *Food Hydrocolloids*, 2001, **15**, 485–490.
45 M. Davidovich-Pinhas and H. Bianco-Peled, *Carbohydr. Polym.*, 2010, **79**, 1020–1027.
46 S. K. Fullerton-Shirey, L. V. N. R. Ganapatibhotla, W. Shi and J. K. Maranas, *J. Polym. Sci., Part B: Polym. Phys.*, 2011, **49**, 1496–1505.
47 Z. Zou, W. J. E. M. Habraken, G. Matveeva, A. C. S. Jensen, L. Bertinetti, M. A. Hood, C.-y. Sun, P. U. P. A. Gilbert, I. Polishchuk, B. Pokroy, J. Mahamid, Y. Politi, S. Weiner, P. Werner, S. Bette, R. Dinnebier, U. Kolb, E. Zolotoyabko and P. Fratzl, *Science*, 2019, **363**, 396–400.
48 B. Thu, P. Bruheim, T. Espevik, O. Smidsrød, P. Soon-Shiong and G. Skjåk-Bræk, *Biomaterials*, 1996, **17**, 1069–1079.